

**UNSTEADY PRESSURE MEASUREMENT OF NACA 0018  
UNDERGOING PURE PITCHING MOTION  
AT DIFFERENT PITCH AMPLITUDES**

By:

**TONG CHEE KENT**

(Matric no: 120592)

Supervisor:

**DR NORIZHAM BIN ABDUL RAZAK**

June 2017

This dissertation is submitted to

Universiti Sains Malaysia

as partial fulfilment of the requirement to graduate with honors degree in  
**BACHELOR OF ENGINEERING (AEROSPACE ENGINEERING)**



School of Aerospace Engineering

Engineering Campus

Universiti Sains Malaysia

# DECLARATION

This work has not previously been accepted in substance for any degree and is not being concurrently submitted in candidature for any degree.

---

**TONG CHEE KENT**

Date: 5 June 2017

## STATEMENT 1

This thesis is the result of my own investigations, except where otherwise stated. Other sources are acknowledged by giving explicit references. Bibliography/references are appended.

---

**TONG CHEE KENT**

Date: 5 June 2017

## STATEMENT 2

I hereby give consent for my thesis, if accepted, to be available for photocopying and for interlibrary loan, and for the title and summary to be made available to outside organizations.

---

**TONG CHEE KENT**

Date: 5 June 2017

# Unsteady Pressure Measurement of NACA 0018 Undergoing Pure Pitching Motion at Different Pitch Amplitudes

Tong Chee Kent

*School of Aerospace Engineering, Universiti Sains Malaysia, 14300 Nibong Tebal, Pulau Pinang*

---

## ABSTRACT

An experimental investigation of the unsteady pressure measurement of a 2D NACA 0018 airfoil oscillating in pitch motion was performed by using pressure transducers at open-circuit wind tunnel. In the case of study, the wind tunnel testing was conducted in low flight regimes ( $Re = 68474$  and  $Re = 136948$ ) at various angles of attack. Static test was performed and the data were obtained as baseline for further analysis. Surface pressure over the lower and upper surfaces of the airfoil was measured and was subsequently used to compute the pressure coefficient. With regard to analysis purpose, for static test, the graphs of pressure coefficient against  $x/c$  of  $2^\circ$ ,  $12^\circ$  and  $18^\circ$  angle of attack at free-stream velocities of  $5\text{ m/s}$  and  $10\text{ m/s}$  were plotted whereas for dynamic test, the 3D representations of pressure distribution with  $x/c$  and time for pitching amplitude of  $5^\circ$ - $15^\circ$  and  $10^\circ$ - $20^\circ$ , pitching frequency of  $3\text{ Hz}$  and free-stream velocities of  $5\text{ m/s}$  and  $10\text{ m/s}$  were plotted.

*Keywords:* unsteady pressure measurement; pitching airfoil; wind tunnel testing

---

## Table of Contents

1. Introduction .....	2
1.1 Evolution of Flapping Wing Aerodynamics.....	3
1.2 Research on Flapping Wing Aerodynamics .....	4
1.3 Computational and Experimental Studies of 2D Pure Pitching Motion.....	4
1.4 Computational and Experimental Studies of 2D Combined Pitching and Flapping Motion.....	5
1.5 Computational and Experimental Studies of Dynamic Stall .....	6
2. Experimental Setup .....	7
2.1 Pitching Wing Model Design .....	7
2.2 Internal Pressure Tapping System .....	9
2.3 Wind Tunnel Testing.....	9
2.4 Calibration Technique .....	10
2.5 Data Acquisition (DAQ).....	11
3. Results and Discussion .....	13
3.1 Steady State Aerodynamic Pressure Measurement (Static Test).....	13
3.2 Unsteady State Aerodynamic Pressure Measurement (Dynamic Test).....	15
4. Conclusion.....	20
Acknowledgements .....	21
References .....	21

## Nomenclature

2D	= Two-dimensional	$P$	= Local pressure
3D	= Three-dimensional	$P_\infty$	= Free-stream pressure
$\alpha$	= Angle of attack	PIV	= Particle Image Velocimetry
$C_p$	= Pressure coefficient	PVC	= Polyvinyl chloride
DAQ	= Data Acquisition	$Re$	= Reynolds number
IMU	= Inertial Measurement Unit	$\rho_\infty$	= Air density
MAVs	= Micro air vehicles	$V_\infty$	= Free-stream velocity
NI	= National Instruments	$x/c$	= Chordwise location

## 1. Introduction

With the advent of the globalization due to the Information Age, flapping wing design has grown gradually in popularity in the early decades. Nowadays, jet-propelled or propeller-driven aircraft is able to cover long distances yet these engines are not agree with the grace and natural power of flying creatures notably birds and insects on the wing. No issue has garnered worldwide attention and interest as the development of flapping flight by virtue of superior aerodynamic efficiency and maneuverability capabilities. The uniqueness of flapping wing design is worth revealing and discovering even though much mystery exists.

In fact, flapping flight can be observed apparently in bird flight. Specialized features like wing bones and feathers contribute tremendously in the flapping flight of birds. The primary feathers on the outer wing are stiff enough to produce forward thrust whereas the secondary feathers on the inner wing are responsible for generating lift by flapping motion. These distinctive wing features have made complicated movements of birds possible as a result of their ability to vary their wing shape in response to individual requirements. On top of that, there are two stages in flapping flight namely upstroke or recovery stroke whereby the wing moves upward and is folded inward to minimize the drag and downstroke or power stroke whereby the wing moves downward and forward to generate thrust.

The underlying idea of bird flight is similar to that of aircraft. When the wings travel through the air, the air is deflected downward as they are held at a certain angle of attack. As a result, the air pressure begins to accumulate below the wings whereas the pressure above the wings is gradually lowered. The pressure difference between top and bottom surfaces of the wing creates a lift force perpendicular to the wing surface and hence this prevents the birds from falling. As a matter of fact, flapping aerodynamic can be investigated in terms of unsteady aerodynamic flow. Larger birds possess low flapping rate while smaller birds and insects flap more by virtue of highly unsteady aerodynamic. The latter has to produce more trailing vortices for the sake of increasing the viscous flow regime [1].

Micro air vehicles (MAVs) have become an indispensable part of flapping wing flight. There are several successful flapping wing MAVs available nowadays. For instance, Percival Spencer developed a significant number of engine-driven ornithopters which resembled a bird. Apart from being a pioneer pilot, he was reckoned as the designer of the Republic Seabee amphibious airplane. He acquired a remarkable achievement in designing the Wham-O Bird which propelled the concept of mechanized flapping wing flight. Besides, Sean Kinkade earned the reputation for producing an

RC ornithopter called Skybird which employed a 0.15 methanol-fueled engine. Electric versions were introduced afterwards. In addition, Robert Musters incorporated foam and twisted wings in the design of RC ornithopters. They were widely applied at airports for bird control purpose [1].

A comprehensive study focused on unsteady flow is recently becoming a matter of the utmost importance. It is an undisputable fact that unsteady flow can create detrimental effects like buffeting, flutter, gust response, vibration and notably dynamic stall [2]. The impact of unsteady flow is considerably profound in a such way that it is recognized as a limiting factor for the high speed performance of airborne aircraft and functioning of mechanical system. For instance, maneuvering aircraft, modern helicopters, flapping wings of birds and insects, wind turbines and many more possess the main concern of unsteady flow with regard to their operations [3].

Countless research, either through computational or experimental approach, has revealed that the unsteady flow can be separating or reattaching on the upper surface of the airfoil. Dynamic stall phenomenon is perceived as the formation and shedding of a vortex in vicinity of the leading edge covering the upper surface of the airfoil. This phenomenon will give rise to a nonlinearly fluctuating pressure field and yield transient variations in forces and moments which are different from those acquired in static stall [2]. The fully separated stall takes place on the upper surface once the leading edge vortex flows past the trailing edge of the airfoil. At the same time, the magnitude of lift and pitching moment diminish abruptly. However, the reattaching of the flow from the leading edge is observed when the angle of attack is lowered. While the occurrence of dynamic stall seems to be destructive to many aircraft, this may be considered a boon for birds and insects as a high lift mechanism with the aid of leading edge vortex induced by the dynamic stall.

For the purpose of continuous study in previous project, the wing motion of an ornithopter incorporates twisting motion instead of flapping motion. Flapping is intimately associated with the plunging motion of the wing in upward and downward directions while twisting involves the pitching motion of the wing along the spanwise axis. Optimization of several governing parameters like flapping angle, flapping frequency and wing geometry is performed. Other than that, wind tunnel test is conducted in which the pressure distribution of a wing undergoing root pitching motion is measured.

### *1.1 Evolution of Flapping Wing Aerodynamics*

A growing amount of interest and research effort in flapping wing design has enabled substantial development in micro air vehicles (MAVs) and submerged vehicles. The tremendous progress in flapping wing flight was attributed to Leonardo da Vinci, who was the inventor of a wing-flapping contraption called ornithopter. Nonetheless, he neglected the production of lift and thrust by the bird wings as the prerequisite to fly, causing the ornithopter failed to work. On top of that, he made his first attempt at publishing a book manuscript entitled “*Sul volo degli Uccelli*” which was chiefly focused on flapping wing studies. The progressive study in developing flapping wing was performed by Otto Lilienthal, the great forerunner in human flight and his brother Gustav in the mid-1800s. Observation of birds flight as well as experimental approaches about flapping wings were the main governing principles of his findings. Lilienthal produced his known work by publishing a book illustrating his experiments and also the energy required in flapping wing flight. Remarkably, he discovered that the cambered airfoil was beneficial in flight compared to flat plate. This preceding discovery by Lilienthal provided the Wright brothers, Orville and Wilbur an insight

in developing powered human flight. They studied the birds flight and grasped that the ability of birds to alter their wing shape aided enhanced maneuverability and hover capabilities. They had made powered flight possible by incorporating this technique to acquire roll control. In 2011, the evolution in flapping flight was evident when the ingenious robot bird, SmartBird by the Festo Corporation appeared to mimic the natural flight of a bird. This flying marvel was capable of performing flight on its own and earned the reputation of increased aerodynamic performance and agility. Apart from moving upward and downward, its sophisticated wings were able to twist at certain angles by virtue of an active articulated torsional drive. SmartBird was also well known for its enhanced resource and energy consumption efficiency as a result of its light weight.

### *1.2 Research on Flapping Wing Aerodynamics*

Extensive research and development on the kinematics of flapping wing pave the way for flying model of flapping flight and its corresponding aerodynamic performance. In the early twentieth century, Knoller [4] and Betz [5] were the first ones to propose the significant finding of an effective angle of attack accompanied with a normal force vector comprising both lift and thrust force components as a result of an oscillating wing undergoing flapping motion. The validation on the preceding Knoller-Betz effect was implemented by Katzmayr [6] in 1922 via a series of tests and experiments. During the test, an airfoil was held stationary in a sinusoidally oscillating wind stream and the resulting thrust force was investigated. In 1935, von Karman and Burgess [7] presented the explanation on drag and thrust generation theoretically which were characterized by the observed location and the orientation of wake vortices. They introduced von Karman Vortex Street by modelling the wake consisting of two rows of alternating vortices across a flapping airfoil in an incompressible flow. On top of that, they distinguished ‘drag producing wake’ and ‘thrust producing wake’ through dye visualizations of wake vortices. In the meanwhile, Theodorsen [8] offered an analytical method in estimating the unsteady aerodynamics force and moment on an oscillating airfoil. Theodorsen’s function was predominated by the inviscid and incompressible flow assumption as well as the Kutta condition at the trailing edge of the airfoil. The approximation of Theodorsen’s function had become an indispensable measure to study airfoil flutter and flapping flight problems. In the mid 1930s, Theodorsen served as an inspiration to Garrick [9] in his way to derive thrust force of an oscillating airfoil in terms of reduced frequency and maximum non-dimensional flapping velocity. He perceived that a plunging airfoil will produce thrust over a wide range of frequency whereas a pitching airfoil merely produced thrust at the upper boundary of critical frequency.

### *1.3 Computational and Experimental Studies of 2D Pure Pitching Motion*

McCroskey [10] conducted a comprehensive study on the significance of unsteady effects in 2D oscillating airfoils in his review. Such unsteady solution with regard to these special and challenging flows were discussed in depth. Nevertheless, the information available now is still insufficient to investigate the relative importance of unsteady flow effects especially the unsteady viscous boundary condition at the wall and the time-varying inviscid pressure gradient [11]. L.E.Ericsson and J.P.Reding [11] experimentally investigated the influence of the mode of oscillation for the airfoil in determining the governing unsteady flow effect. F.Ajalli, M.Mani and M.R.Soltani [12] performed experiments to measure the pressure distribution on a 2D heaving E361 airfoil in a subsonic wind tunnel. In contrast with preceding experiments, M.R.Soltani, M.Mani and E.Tolouei [13] experimentally studied the aerodynamic behavior of a 2D E361 airfoil undergoing

high pitching motion in an incompressible regime. The experiments were designed to study the unsteady surface pressure measurement on a pitching airfoil.

McCroskey et al. [14], from their experiments, revealed that the compressibility was the key parameter in determining pitching airfoil performance. They deduced that as the angle of attack of an airfoil increases, the flow velocities in vicinity of the leading edge increase four to five times higher than the free-stream velocity. McAlister, Pucci, McCroskey and Carr [15] carried out an experimental investigation on eight airfoil profiles at various subsonic free-stream velocities and sinusoidal pitching oscillation. In addition to pressure distribution, other outcomes including the lift, drag and pitching moment were obtained. Fung and Carr [16] observed the flow behavior around a NACA 0012 airfoil undergoing pure pitching motion with  $15^\circ$  mean angle of attack and  $10^\circ$  pitching amplitude prior to flow separation. They discovered that for subcritical flows, the airfoil was able to achieve larger maximum suction at high angle of attack as result of the separation of boundary layer was delayed due to an increase in reduced frequency. On the other hand, for supercritical flows, the local outer flow and the boundary layer were not stable because of the growing of the flow vortices in vicinity of the leading edge.

Garrick [9], in his finding, proved that pure pitching motion was not ideal for thrust generation since it will merely generate positive thrust by employing high frequencies. This result was being validated by Koochesfahani [17] via a number of experimentation. By applying a 2D discrete vortex method, Sarkar and Venkatraman [18] studied numerically the flow over an airfoil undergoing pure pitching motion. From their results, they verified that the mean angle of attack and pitch axis location had a profound effect on the thrust generation.

#### *1.4 Computational and Experimental Studies of 2D Combined Pitching and Flapping Motion*

Long and Fritz [19] proposed the unsteady vortex lattice method in order to model the flapping, oscillating, pitching, plunging and twisting motion of a finite wing with certain aspect ratio. The model developed encompassed free-wake relaxation, vortex dissipation effects and vortex stretching. Knut Streitlien et al. [20] performed a research on the flow with a uniform velocity field accompanied by vortices over a combined pitching and heaving hydrofoil. They revealed that the phase between hydrofoil motion and flow vortices was a prerequisite to the 2D inviscid analysis. DeLaurier and Harris [21] experimentally investigated the flapping wing oscillating in varying pitching amplitude and phase angle in a subsonic wind tunnel. The outcome would be the plot of average thrust coefficient against reduced frequency with various pitching amplitude and phase angle. Razak and Dimitriadis [22] conducted the experimental investigation of mechanical wings undergoing pitching and flapping motion in the wind tunnel. The experiment was designed to study the influence of pitch angle oscillations and wing profile on the aerodynamic forces produced. A wide range of parameters including airspeed, geometric angle of attack, pitching and flapping kinematics, reduced frequency and wing sections were varied to determine the effect on aerodynamic forces. They also deduced that the Reynolds number was known as the influential parameter for the aerodynamic forces depending on the camber of the wings.

By applying 2D compressible Navier-Stokes solver, Tuncer et al. [23] studied the flow over a 2D NACA 0012 airfoil oscillating in pitch and flap motion. They discovered that for all values of reduced frequency, the flapping motion lagged the pitching motion by a phase difference of  $90^\circ$  in the propulsive efficiency. Two years later, Tuncer and Platzer [24] investigated the influence of

dynamic stall on the propulsive efficiency and thrust force using similar method. They deduced that there was a sudden decline in propulsive efficiency once the dynamic stall phenomenon occurred. Isogai et al. [25] conducted Navier-Stokes simulations of flow over a combined pitching and flapping airfoil with NACA 0012 profile. They perceived that the propulsive efficiency decreased rapidly as soon as dynamic stall occurred. Anderson et al. [26] experimentally investigated the effect of Strouhal number on the propulsive efficiency and thrust force of a combined pitching and flapping airfoil with NACA 0012 profile. It was concluded that the propulsive efficiency was highly dependent on the phase angle between pitching and flapping motion. With the aid of numerical solution of the vorticity equation, Guglielmini and Blondeaux [27] studied the effect of various flapping parameters on the propulsive efficiency of a combined pitching and heaving elliptic foil. These parameters included pitching amplitude, maximum non-dimensional flapping velocity, phase angle between pitching and flapping motion and the pivot position of the pitching axis. Via a finite element incompressible Navier-Stokes solver, Ramamurti and Sandberg [28] numerically simulated the flow over a NACA 0012 airfoil undergoing flapping motion. They stated that the maximum non-dimensional flapping velocity was the primary driver for the thrust generation. Read et al. [29] and Schouveiler et al. [30] conducted experiments to study the effect of different pitch amplitude and maximum non-dimensional flapping velocity on the flow over a NACA 0012 airfoil oscillating in pitch and flap motion. They highlighted that incorporating a mean pitching angle can offer a strong side force which eased the maneuver.

### *1.5 Computational and Experimental Studies of Dynamic Stall*

Ericsson and Reding [31] performed extensive studies on dynamic stall phenomenon which applied a quasi-steady theory that required static experimental data for estimating the dynamic stall. McCroskey [32] investigated the inviscid flow field of an unsteady airfoil notably on the dynamic stall region. His analysis was based on the velocity potential in the unsteady wake of an oscillating wing by taking angle of attack, camber and thickness into account to determine the pressure distribution around the wing. He deduced that the boundary layer separation can be predicted by the assumption of inviscid flow. Several years later, McCroskey [10] contributed to offering the physical behavior and interpretations of dynamic stall phenomenon. He highlighted that the negative damping effects were crucial in the cycle of motion such that the resulting force can be larger at a specific angle of attack than that at a sufficiently high angle of attack. The flow field around the wing would drive the formation of dynamic stall.

Tran and Petot [33] successfully built the ONERA semi-empirical model for 2D dynamic stall of an airfoil. This model used curve fitting to experimental data to analyze the aerodynamic forces as an important parameter characterizing the wing motion. Bielawa et al. [34] also created a semi-empirical model which aided in analyzing the fluid dynamic forces using the pitch and pitch rate of the wing.

Via vortex method, Akbari and Price [35] performed a numerical simulation on 2D elliptic airfoils undergoing pitching motion with high mean angles of attack in an incompressible viscous flow. The simulation served the purpose of observing the effects of frequency of oscillation, location of pitch axis, mean angle of attack and thickness ratio of airfoil on the flow pattern in the region of dynamic stall. They stated that the reduced frequency possessed the greatest effect on the flow field. After years of hard work, Akbari and Price [36] applied the similar method to simulate the flow

around a NACA 0012 airfoil oscillating in pitch motion. Likewise, they drew an inference indicating that the flow field was highly influenced by the reduced frequency.

By employing the Particle Image Velocimetry (PIV) technology, Wernet et al. [37] performed their research in the flow field of a pitching airfoil under dynamic stall conditions. They identified that the flow field was characterized by high degree of nonreproducibility in terms of vortex structure geometry in the cycle of motion. The nonreproducibility trait was said to be dominated by the reduced frequency.

## **2. Experimental Setup**

In this section, the experimental procedure accompanied by the apparatus and devices used in four main stages encompassing design, fabrication, assembly and wind tunnel testing is outlined in detail. The wind tunnel testing is carried out in Aerodynamic Laboratory located at School of Aerospace Engineering, Universiti Sains Malaysia. An open-circuit wind tunnel which possesses the test section dimension of 550 mm length, 350 mm width and 460 mm height is employed. The fan system in this tunnel is capable of producing a maximal airspeed of 17 m/s or equivalent to 2600 rpm. The pitching wing model is placed in the test section to allow the air flowing over it for the measurement of the aerodynamic properties.

In order to explore the study of pitching wing more thoroughly, the wind tunnel testing is conducted in terms of steady state aerodynamic pressure measurement (static test) and unsteady state aerodynamic pressure measurement (dynamic test). With regard to static test, the wind tunnel testing serves the purpose of measuring the pressure distribution of a pitching wing at different angle of attack from  $0^\circ$  to  $20^\circ$  with an increment of  $2^\circ$ . On the other hand, dynamic test involves determining unsteady pressure measurement of a wing undergoing twisting wing motion in four different cases; the pitching angles vary from  $-5^\circ$  to  $5^\circ$ , from  $0^\circ$  to  $10^\circ$ , from  $5^\circ$  to  $15^\circ$  and from  $10^\circ$  to  $20^\circ$  angle of attack. The experiment commences with the free-stream velocity of 5 m/s and proceeds with an increased two-fold free-stream velocity of 10 m/s; both these free-stream velocities correspond to low flight regimes or low Reynolds number.

### *2.1 Pitching Wing Model Design*

Preliminary design of the pitching wing model is depicted in Figure 1. For the sake of facilitating the mounting of wing in the wind tunnel test section, alteration and modification have been made on the wing design, resulting in the fabricated wing design shown in Figure 2. With reference to Figure 2, the straight conventional wings with symmetrical airfoil of NACA 0018 profile is chosen for the wing design by virtue of its ease of fabrication. The wing design features a semi-wingspan of 0.200 m and a chord length of 0.200 m. Relevant wing geometry and mass are tabulated in Table 1 below.

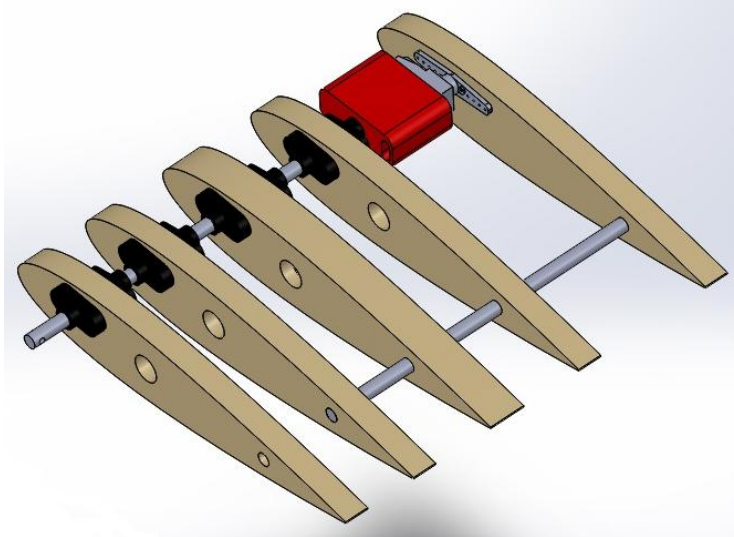


Figure 1: Preliminary design of pitching wing model

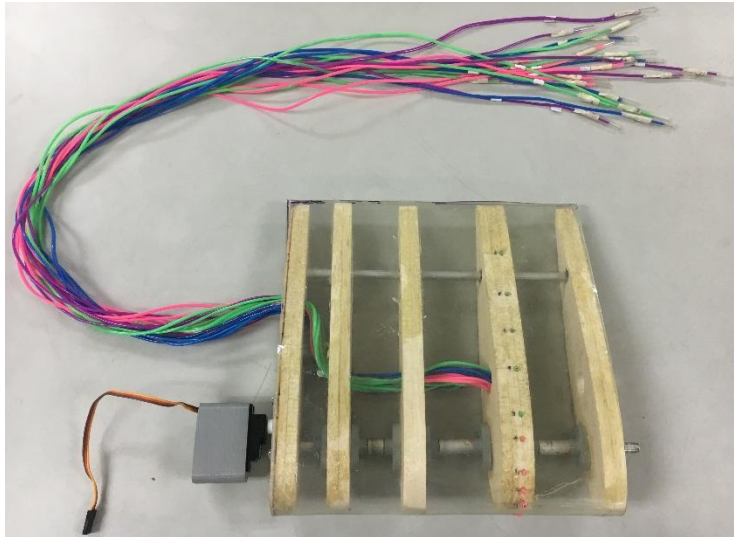


Figure 2: Fabricated design of pitching wing model

Table 1: Wing geometry and mass

Semi-Wingspan (m)	Chord Length (m)	Semi Wing Area (m <sup>2</sup> )	Aspect Ratio	Mass (g)
0.200	0.200	0.040	2	291.5

Generally speaking, the pitching wing model is composed chiefly of ribs, front and rear spars, rib-spar supports, servo, servo holder and some standard parts. A total number of five ribs is constructed using balsa wood due to its superior strength-to-weight ratio and ease in handling. The lightweight construction also paves the way for mitigating and minimizing the occurrence of vibration on the wing itself. One rib is exclusively made hollow in order to install internal pressure tapping system used for pressure measurement purpose. There are two solid aluminium rods working as front and rear spars which contribute in resisting the applied bending load. Apart from this, skinning of the wing model is done by coating the entire wing with a layer of flexible polyvinyl chloride (PVC); it is designed to impart an aerodynamic surface for the wing model. A rectangular aluminium plate of small dimension is attached on one of the ribs together with the servo. Via this,

the pitching forces tend to be uniformly distributed throughout the ribs and therefore this facilitates the pitching motion of the wing.

An analog servo modelled HD-1160A is incorporated in the wing design to govern and take control of pitching wing motion along the spanwise axis. The servo is controlled by Arduino Uno R3 microcontroller connected to personal computer to adjust a specified angle of attack and provide desirable pitching movement for the wing in static test and dynamic test respectively. Besides, a rectangular block of pressure sensor accommodating several pressure transducers is introduced to convert the pressure acting on the wing into electrical signals in voltage form. The preceding electrical signals are digitized by National Instruments USB-6001 Data Acquisition (DAQ) connected to the pressure sensor and the personal computer. On top of that, pertaining to unsteady state aerodynamic pressure measurement, a 5V 5 DOF Gyro Accelerometer Inertial Measurement Unit (IMU) is attached on the wing skin in the vicinity of trailing edge; it is designed to register a definite pitching angle at each instantaneous time and obtain the pitching frequency of the wing. This accelerometer sensor is connected to National Instruments USB-6009 Data Acquisition (DAQ) which acts as the interface between electrical signals from the sensor and personal computer.

## 2.2 Internal Pressure Tapping System

In the case of study, there are all 19 pressure tapings covering the surfaces of the pitching wing model as indicated in Figure 3. These pressure tapings are located along the lower and upper surfaces of hollow rib which encompass nine tapings on both the lower and upper surfaces and one at the stagnation point (leading edge). Each pressure tapping is installed and numbered accordingly relative to the position on the chord length of the wing; the numbering system of 0, 1/18, 2/17, 3/16, 4/15, 5/14, 6/13, 7/12, 8/11 and 9/10 exhibits the symmetrical distribution of pressure tapings throughout the surfaces of the wing. A significant number of long silicone tube is inserted into these pressure tapings and subsequently connected to the pressure ports of pressure sensor. The pressure readings obtained from each port reveal the pressure coefficient generated on each predetermined pressure tapping during the pitching motion of the wing.

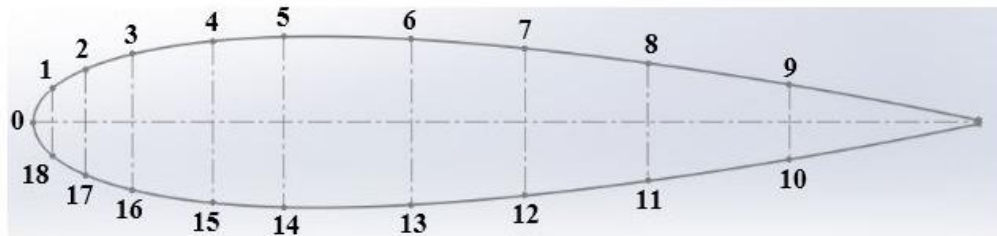


Figure 3: Pressure tapings location on NACA 0018 airfoil

## 2.3 Wind Tunnel Testing

In this instance, wind tunnel testing is designed to investigate the aerodynamic performance of pitching wing at various free-stream velocities. As evidenced by the experimental setup shown in Figure 5, this section primarily focuses on the experimental procedure and precautions taken in conducting the wind tunnel testing. The wing model is mounted firmly in the wind tunnel test section in vertical position so as to eliminate the gravitational effect acting on the wing. An additional styrofoam is used to further strengthen the mounting of the wing and restrict the undesired movement or vibration. Failure of securing the wing firmly will lead to inaccuracies in pressure measurement. The hatch of the wind tunnel test section is then closed properly to avoid

affecting the air flow. Prior to commencing the experiment, several precautions notably inspection tasks are taken to prevent incorrect data measurement. These include checking the connections of the apparatus and devices and checking the workability of the pressure transducers. The wing model is subsequently allowed to undergo pitching motion after the coding program is uploaded to the Arduino microcontroller. The wind tunnel is switched on and the fan speed is adjusted to 840 rpm and 1560 rpm for free-stream velocity of 5 m/s and 10 m/s respectively. Once the steady air flow is achieved, the dynamic pressure reading on the pitot tube anemometer and differential manometer is taken as well as the pressure readings displayed on the computer screen are recorded.

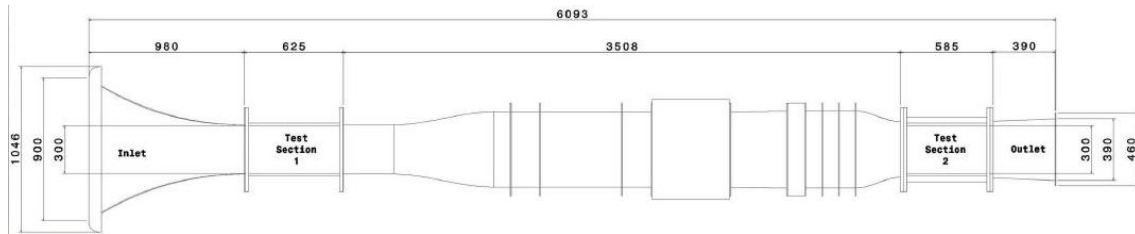


Figure 4: Schematic diagram of open-circuit wind tunnel

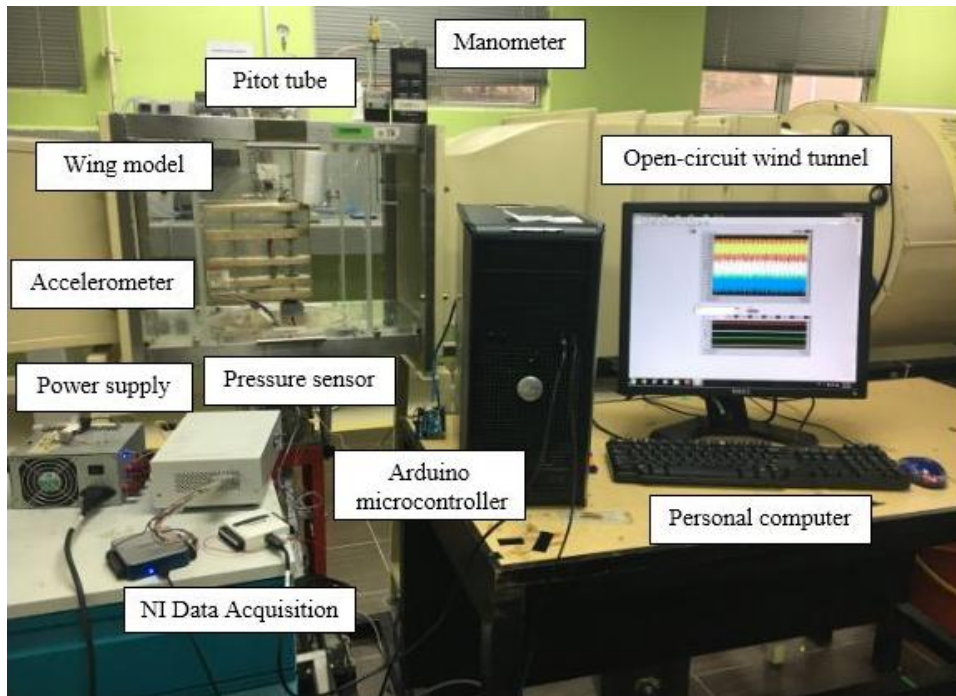


Figure 5: Experimental setup

## 2.4 Calibration Technique

In lieu of voltage reading, pressure reading is the governing parameter in the experiment. As a result, a simple calibration technique is demonstrated in order to investigate the relationship between voltage and pressure. In other words, this method is designed for the conversion from voltage reading into pressure reading by means of a gradient value. Pertaining to calibration setup shown in Figure 6, two small tied tubes of pressure sensor and manometer are placed at the same water level to yield voltage and pressure readings respectively. The measurements are taken at different water position for maximizing the accuracy of the results. Subsequently, the results are

represented in a graphical form whereby the pressure reading is plotted against the voltage reading. As depicted in Figure 7, the calibration curve displays the linear function of two variables with a negative slope. The negative value of the gradient of -1135 is then inserted into the block diagram in NI LabVIEW software for the conversion purpose.



Figure 6: Calibration setup

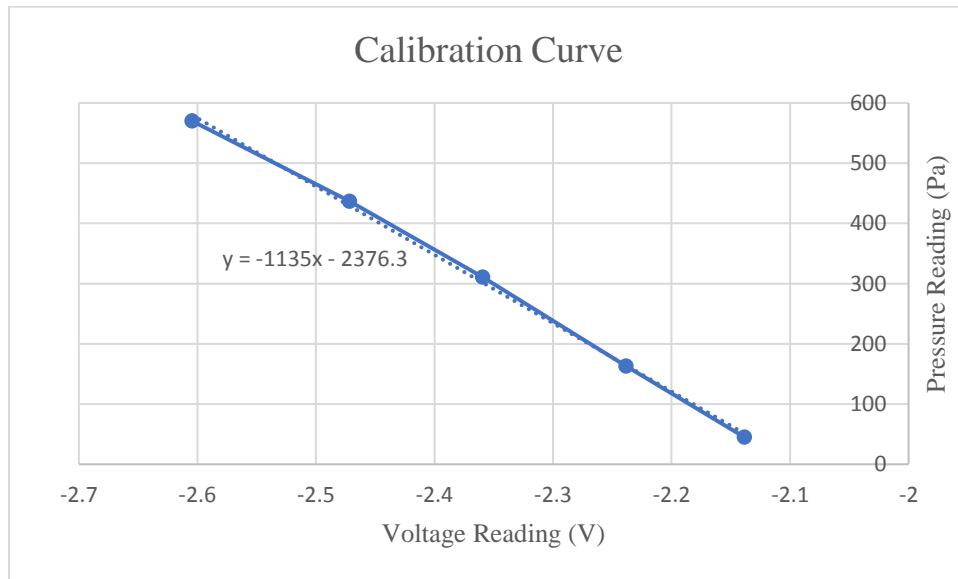


Figure 7: Graph of pressure reading against voltage reading

### 2.5 Data Acquisition (DAQ)

Under unsteady state aerodynamic pressure measurement, the Data Acquisition (DAQ) system consists of sensors, DAQ measurement hardware and a personal computer. The DAQ system is predetermined such that it is capable of obtaining 2000 samples of data within one second. In the experiment, the pressure transducers produce electrical signals in voltage form which continuously vary over time while National Instruments DAQ performs the function of DAQ for the pressure measurement. At the same time, another National Instruments DAQ is introduced to record the instantaneous pitching angle for a period of time. Via NI LabVIEW software, a block diagram is

built for processing and storing the measurement data. Examples of block diagram being used in static test and dynamic test are shown in Figure 8 and Figure 9 respectively. The data obtained is equivalent to pressure reading after the negative gradient value from the calibration curve is added to the block diagram. After subtracting from the initial value, the new pressure values form the numerator of the mathematical formula of pressure coefficient. The pressure coefficient, a dimensionless quantity, is given by

$$C_p = \frac{p - p_\infty}{\frac{1}{2} \rho_\infty V_\infty^2} \quad (1)$$

where  $p$  is the local pressure,  $p_\infty$  is the free-stream pressure,  $\rho_\infty$  is air density and  $V_\infty$  is the free-stream velocity. The raw data obtained in DAQ is subsequently imported to Matlab software for generating the graphs showing the pressure distribution acting on both the lower and upper wing surfaces at various free-stream velocities.

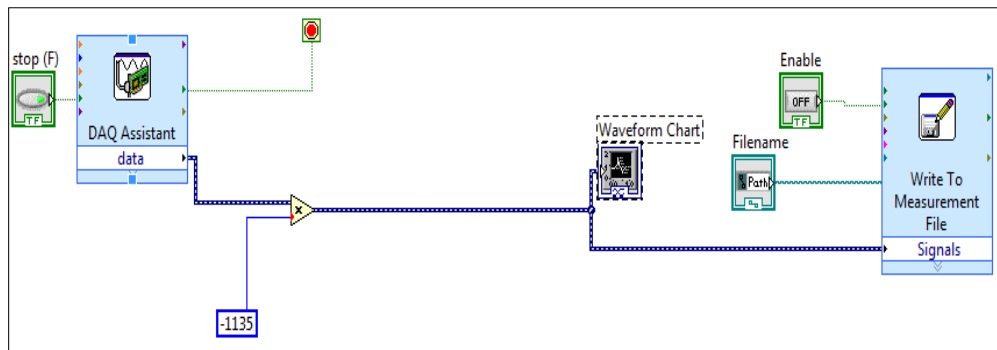


Figure 8: Block diagram for static test

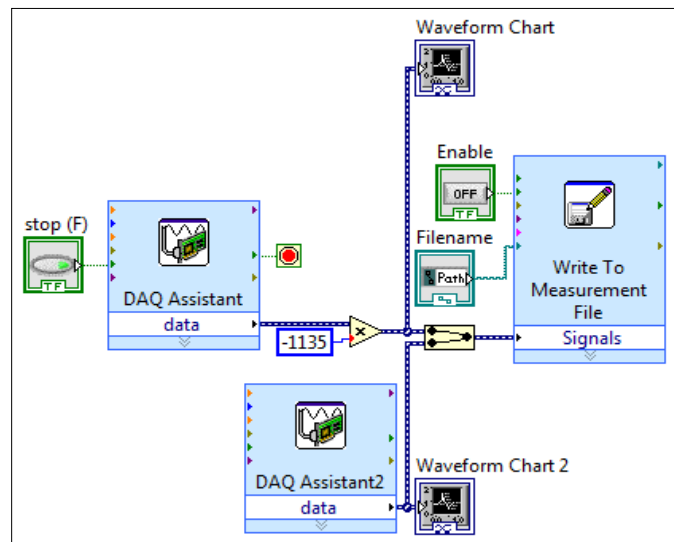


Figure 9: Block diagram for dynamic test

### 3. Results and Discussion

#### 3.1 Steady State Aerodynamic Pressure Measurement (Static Test)

Pertaining to static test, the experimental investigation is conducted on the pitching wing model which is held still with a predetermined angle of attack. For analysis purpose, the aerodynamic characteristics of the NACA 0018 airfoil is evaluated and examined in terms of pressure coefficient. In order to give a clearer vision for comparison,  $2^\circ$ ,  $12^\circ$  and  $18^\circ$  which correspond to low, moderate and high angles of attack are presented in the pressure variation plot. Airspeed is also varied to study its effect on the pressure distribution over the lower and upper surfaces of the wing. The wind tunnel testing is performed in low flight regime with the Reynolds number of 68474 and 136948. Table 2 shows the tabulation of results of pressure coefficient over the wing surfaces at various angles of attack for different free-stream velocity.

Table 2: Pressure coefficient over the upper and lower surfaces of NACA 0018 airfoil at  $\alpha = 2^\circ, 12^\circ$  and  $18^\circ$  for  $V_\infty = 5 \text{ m/s}$  and  $10 \text{ m/s}$

No	$x/c$	$C_p$					
		$V_\infty = 5 \text{ m/s}$			$V_\infty = 10 \text{ m/s}$		
		$\alpha = 2^\circ$	$\alpha = 12^\circ$	$\alpha = 18^\circ$	$\alpha = 2^\circ$	$\alpha = 12^\circ$	$\alpha = 18^\circ$
0	0.000	1.0000	0.4504	-0.0460	0.7312	0.6043	-0.1421
1	0.020	-0.6676	0.7501	1.0000	-0.9075	0.2843	0.7895
2	0.055	-1.1819	0.1392	0.5344	-0.7102	-0.1834	0.1769
3	0.105	-0.7203	0.2090	0.4467	-0.8296	-0.3091	0.0435
4	0.190	-1.0692	-0.4100	-0.1975	-1.0193	-0.4949	-0.2706
5	0.265	-0.7234	-0.1945	0.0913	-0.8593	-0.5572	-0.3210
6	0.400	-0.5211	-0.1448	0.0326	-0.5362	-0.4134	-0.2571
7	0.520	-0.5528	-0.2076	-0.0812	-0.6771	-0.4673	-0.4477
8	0.650	-0.6654	-0.3278	-0.2773	-0.7986	-0.4551	-0.4155
9	0.800	-0.0310	0.1253	0.1717	-0.1340	-0.1511	-0.0580
10	0.800	-0.2138	-0.1437	0.0386	-0.1821	-0.2549	-0.2701
11	0.650	-0.2494	-0.4413	-0.2056	-0.3143	-0.3254	-0.3129
12	0.520	-1.3049	-1.3074	-1.3594	-1.3609	-1.2574	-1.3369
13	0.400	-0.9387	-0.9935	-1.0040	-1.3291	-1.2850	-1.3837
14	0.265	-0.8389	-0.7370	-0.9372	-1.1761	-1.3510	-1.3301
15	0.190	-0.8099	-0.8295	-1.0024	-1.1197	-1.3945	-1.5041
16	0.105	-0.5225	-0.9306	-1.0783	-0.7207	-0.9616	-1.1551
17	0.055	-1.0295	-1.8381	-1.8616	-1.5830	-2.4602	-3.0647
18	0.020	-0.8763	-2.3781	-2.9855	-1.1332	-2.4027	-3.5447

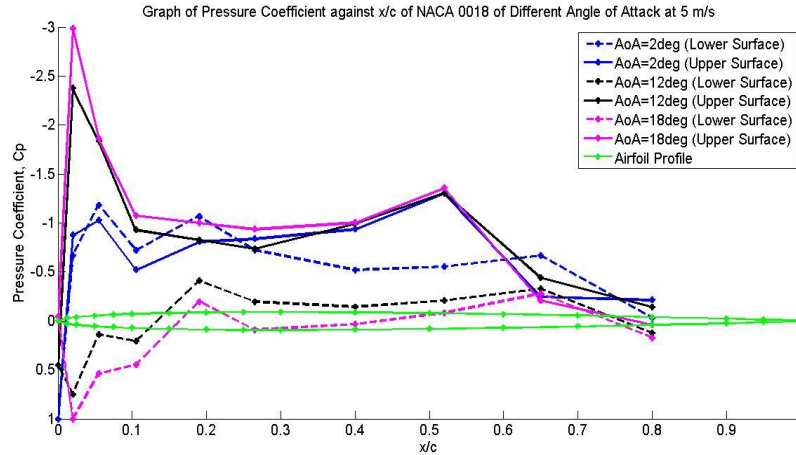


Figure 10: Distribution of pressure coefficient over the lower and upper surfaces of an NACA 0018 airfoil of different angle of attack at 5 m/s

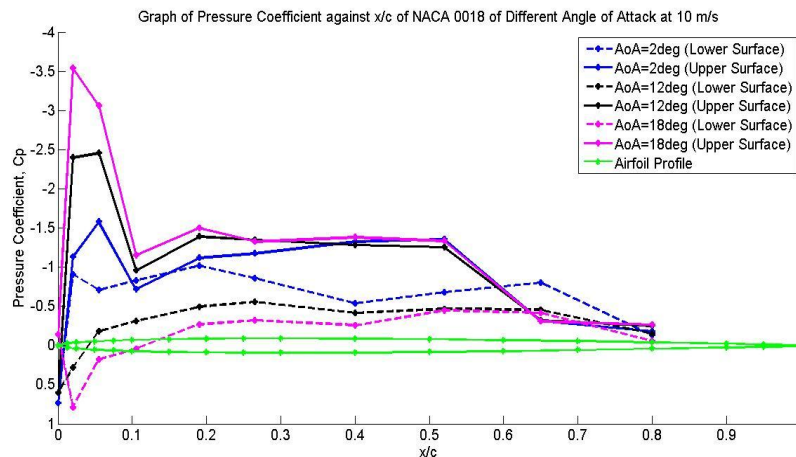


Figure 11: Distribution of pressure coefficient over the lower and upper surfaces of an NACA 0018 airfoil of different angle of attack at 10 m/s

Figure 10 and Figure 11 illustrate the pressure distribution of an NACA 0018 airfoil of different angle of attack at free-stream velocities of 5 m/s and 10 m/s respectively. The pressure distribution curves in both figures exhibit similar shape in which the magnitude of pressure coefficient on the upper surface is smaller than that on the lower surface. With reference to the figures above, the pressure coefficient at the stagnation point (leading edge) is positive since the local pressure is greater in magnitude than the free-stream pressure except for the case of  $18^\circ$  angle of attack. However, there is a downward trend in local pressure as the flow expands throughout the upper surface of the airfoil, resulting in the negative values of pressure coefficient in those regions.

At  $2^\circ$  angle of attack, indicated by blue line, the pressure distribution over the upper surface is similar to that over the lower surface. However, at  $12^\circ$  and  $18^\circ$  angles of attack, indicated by black and purple line respectively, the pressure distribution over the upper surface is relatively smaller than that over the lower surface. It is because at high angles of attack, the stream tube senses the upper portion of the airfoil as an obstruction due to a decrease in cross-sectional area and therefore the flow velocity on the upper surface increases. On the other hand, the flow velocity on the lower

surface decreases because of fewer effect of an obstruction. Since the air is incompressible due to low subsonic speed of airflow in wind tunnel, Bernoulli's equation can be applied which dictates the static pressure decreases as the flow velocity increases and vice versa, leading to smaller pressure distribution over the upper surface [38]. The large pressure difference between the upper and lower surfaces of the airfoil creates a lift force, which is perpendicular to the relative wind, in the upward direction. Therefore, it can be deduced that the flow remains attached at high angles of attack. Remarkably, the pressure difference at  $12^\circ$  angle of attack is not as much as that at  $18^\circ$  angle of attack, implicitly showing that the flow field is still attaching to the upper surface on the forward portion of the airfoil albeit at high angle of attack. This holds the truth in both cases for free stream velocities of 5 m/s and 10 m/s.

In comparison with both figures, the pressure distribution curves with higher free-stream velocity shift upwards to a smaller value. In other words, for free-stream velocity of 10 m/s, a minimum value of pressure coefficient of -3.5447 is registered by the NACA 0018 airfoil at  $18^\circ$  angle of attack. This phenomenon can be explained in terms of mathematical expression. Using equation (1), higher free-stream velocity contributes to a larger magnitude of dynamic pressure and hence lowering the pressure coefficient.

### 3.2 Unsteady State Aerodynamic Pressure Measurement (Dynamic Test)

For dynamic test, the wing model is allowed to oscillate in dynamic pitching motion which is dominated by the program uploaded to the Arduino microcontroller. The flow behavior over the pitching NACA 0018 airfoil is investigated based on the variation of unsteady aerodynamic pressure with chordwise location and time. The outcomes are displayed in 3D plot of the three aforementioned governing parameters so as to gain an insight into the flow pattern of a pitching airfoil. There are all 4 different cases in dynamic test encompassing variable pitching amplitude of  $5^\circ - 15^\circ$  and  $10^\circ - 20^\circ$  as well as free-stream velocity of 5 m/s and 10 m/s.

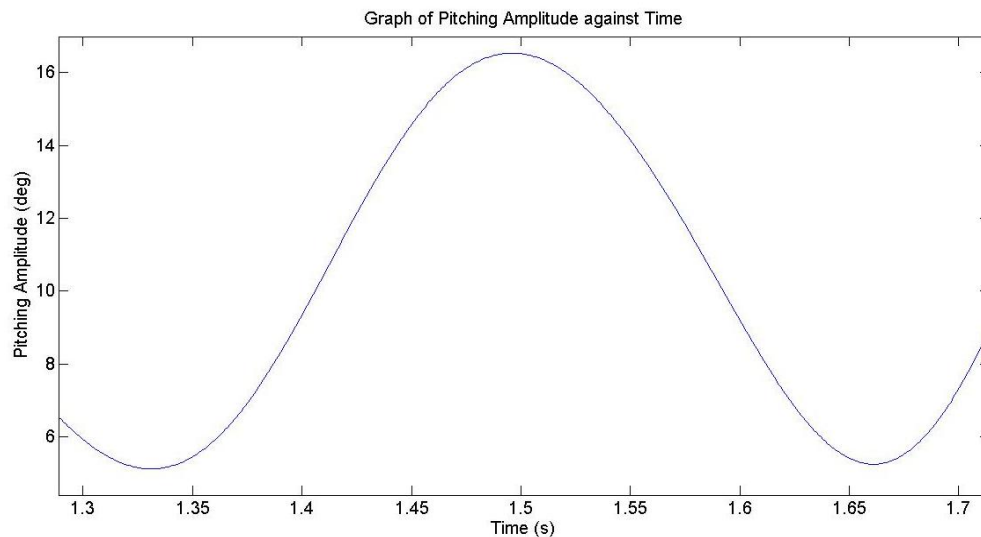


Figure 12: Graph of pitching amplitude against time  
(Pitching amplitude =  $5^\circ - 15^\circ$ , Free-stream velocity = 5 m/s)

Figure 12 shows the graph of pitching amplitude against time for pitching amplitude =  $5^\circ - 15^\circ$  and free-stream velocity = 5 m/s. It can be inferred that the pitching amplitude curve exhibits sinusoidal

pattern as the time travels. The variation of pitching amplitude is constantly steady along the time axis. Via this, the pitching frequency of the wing model can be estimated. In a similar fashion, this sinusoidal variation is also true for other cases of different pitching amplitude or free-stream velocity yet the figures are different.

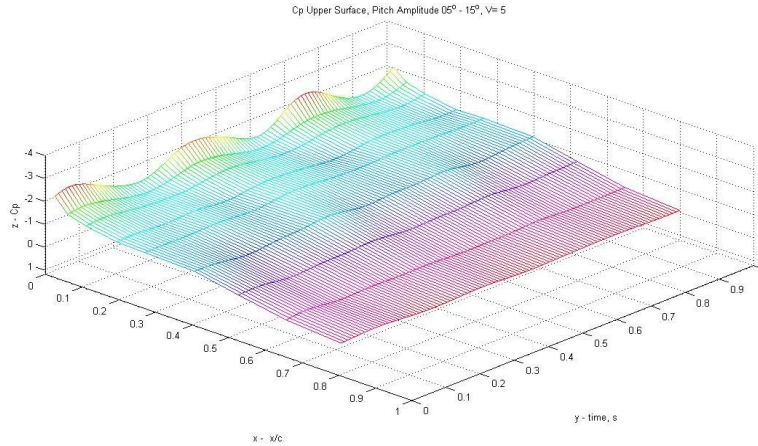


Figure 13: Variations of pressure coefficient with chordwise location on upper surface of NACA 0018 airfoil and time (Pitching amplitude =  $5^\circ - 15^\circ$ , Pitching frequency = 3 Hz, Free-stream velocity = 5 m/s)

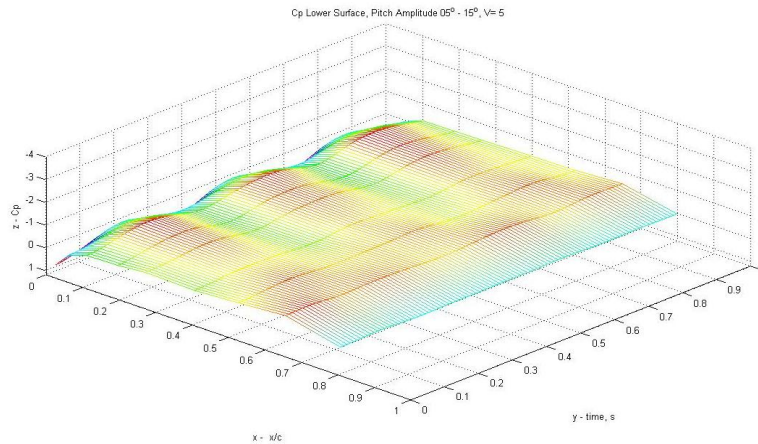


Figure 14: Variations of pressure coefficient with chordwise location on lower surface of NACA 0018 airfoil and time (Pitching amplitude =  $5^\circ - 15^\circ$ , Pitching frequency = 3 Hz, Free-stream velocity = 5 m/s)

Figure 13 and Figure 14 depict the dynamic variations of pressure coefficient with chordwise location on upper and lower surfaces and time for pitching amplitude =  $5^\circ - 15^\circ$ , pitching frequency = 3 Hz and free-stream velocity = 5 m/s. Moving across the time, there is a minimum pressure coefficient called suction peak, indicated by red colour, in vicinity of the leading edge of the airfoil. It is then accompanied by a region of increasing static pressure (adverse pressure gradient) up to the trailing edge of the airfoil. Remarkably, leading edge stall is expected to occur as evidenced by the fact that the maximum suction is lowered to a great extent. When the airfoil pitches to a sufficiently high angle of attack, the pressure variation is marginal which implies that a fully developed stall occurs at the instant in time.

Moving across the chordwise location, the variations of pressure coefficient with time resemble a sinusoidal function. It is obvious that near the leading edge of the airfoil, there is a dramatic rise in pressure coefficient as the angle of attack increases [2]. On top of that, the pressure variation on

the forward portion of the airfoil is different from that on the aft portion one. In the former case, the variation of pressure coefficient with time is consistent with the variation of angle of attack. In other words, the flow field on the forward portion of the airfoil is still attached to the upper surface. However, in the latter case, the variation of pressure coefficient becomes negligible and the flow is separating at  $x/c = 0.5$  on the aft portion of the airfoil.

On the other hand, it can be inferred that lower surface does not garner any point of interest; lower surface exhibits a lower pressure variation compared to the upper surface. The pressure variation is insignificant in vicinity of the trailing edge of the airfoil irrespective of time.

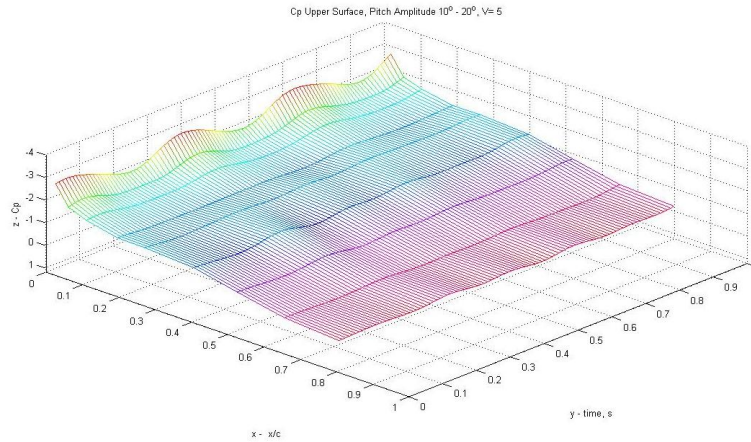


Figure 15: Variations of pressure coefficient with chordwise location on upper surface of NACA 0018 airfoil and time (Pitching amplitude =  $10^\circ - 20^\circ$ , Pitching frequency = 3 Hz, Free-stream velocity = 5 m/s)

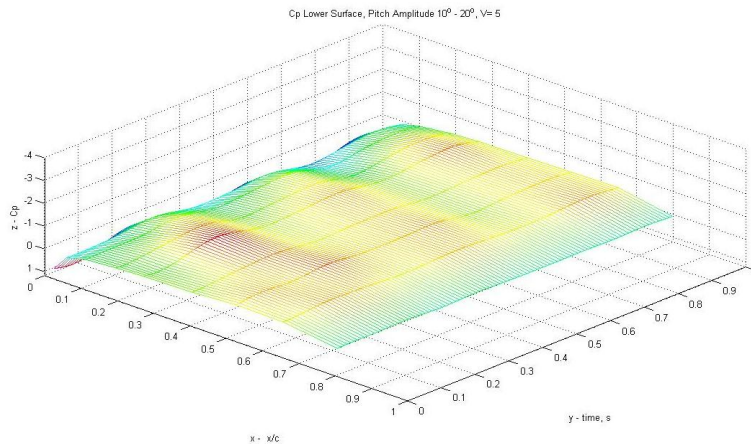


Figure 16: Variations of pressure coefficient with chordwise location on lower surface of NACA 0018 airfoil and time (Pitching amplitude =  $10^\circ - 20^\circ$ , Pitching frequency = 3 Hz, Free-stream velocity = 5 m/s)

Figure 15 and Figure 16 illustrate the dynamic variations of pressure coefficient with chordwise location on upper and lower surfaces and time for pitching amplitude =  $10^\circ - 20^\circ$ , pitching frequency = 3 Hz and free-stream velocity = 5 m/s. Moving across the time, when the pitching amplitude increases, the adverse pressure gradient on the upper surface shown in Figure 15 also increases, which is relatively larger than that in Figure 13. The pressure grows at a rapid rate in the downstream direction. At a specified angle of attack, the presence of a strong adverse pressure gradient causes the boundary layer to separate from the upper surface.

Moving across the chordwise location, in contrast with minimum pressure coefficient of -2.1 in Figure 13, the suction peak on the upper surface records a smaller value of pressure coefficient of -2.6 in Figure 15. Apart from this, the flow separation is deemed to take place ahead of  $x/c = 0.5$  by virtue of its minimal variation of pressure coefficient. Therefore, it can be deduced that increasing the pitching amplitude tends to amplify the maximum suction and accelerate the flow separation.

In a similar fashion, there is no significant information extracted from the lower surface plot in Figure 16 since the pressure variation on the lower surface of the airfoil can be ignored.

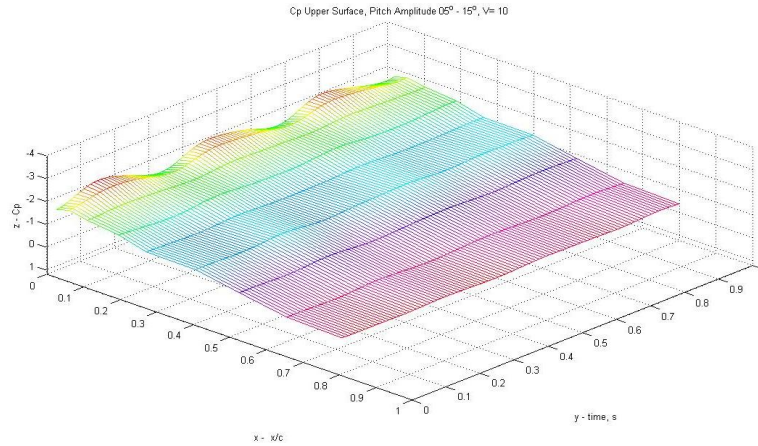


Figure 17: Variations of pressure coefficient with chordwise location on upper surface of NACA 0018 airfoil and time (Pitching amplitude =  $5^\circ - 15^\circ$ , Pitching frequency = 3 Hz, Free-stream velocity = 10 m/s)

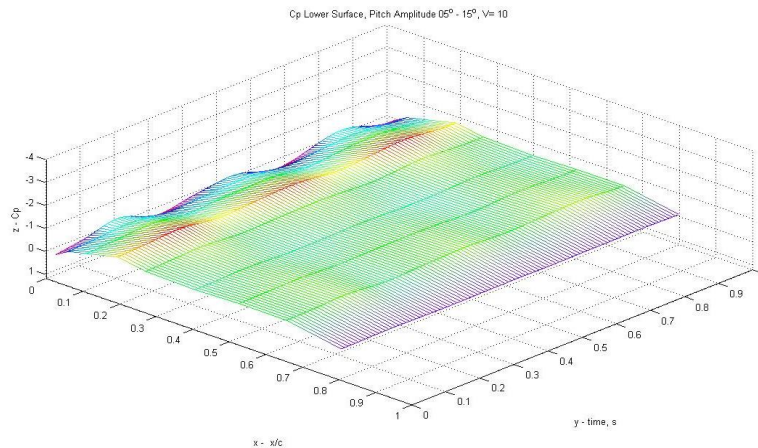


Figure 18: Variations of pressure coefficient with chordwise location on lower surface of NACA 0018 airfoil and time (Pitching amplitude =  $5^\circ - 15^\circ$ , Pitching frequency = 3 Hz, Free-stream velocity = 10 m/s)

Figure 17 and Figure 18 show the dynamic variations of pressure coefficient with chordwise location on upper and lower surfaces and time for pitching amplitude =  $5^\circ - 15^\circ$ , pitching frequency = 3 Hz and free-stream velocity = 10 m/s. Moving across the time, higher free-stream velocity has gradually reduced the maximum suction on the upper surface. It is apparently true when the suction peak registers a slight increased value of pressure coefficient. Other than that, the adverse pressure gradient is not governed by free-stream velocity, indicating that the adverse pressure gradient remains steady even though the free-stream velocity is doubled.

Moving across the chordwise location, the sinusoidal variation of pressure coefficient with time in Figure 17 is lagging compared to that in Figure 13. In other words, the pressure is initially low in position and subsequently climbs to the suction peak as the angle of attack increases. Remarkably, free-stream velocity possesses a profound effect on the occurrence of flow separation. Flow separation is moved forward such that the flow starts to separate at  $x/c = 0.2$  on the forward portion of the airfoil due to its minimal pressure variation.

Likewise, the pressure variation on the lower surface is less than that on the upper surface. The former one exhibits an unchanging pattern regardless of chordwise location and time.

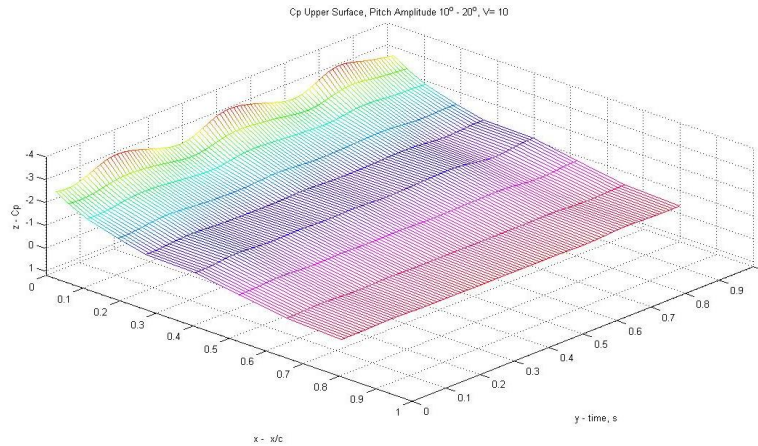


Figure 19: Variations of pressure coefficient with chordwise location on upper surface of NACA 0018 airfoil and time (Pitching amplitude =  $10^\circ - 20^\circ$ , Pitching frequency = 3 Hz, Free-stream velocity = 10 m/s)

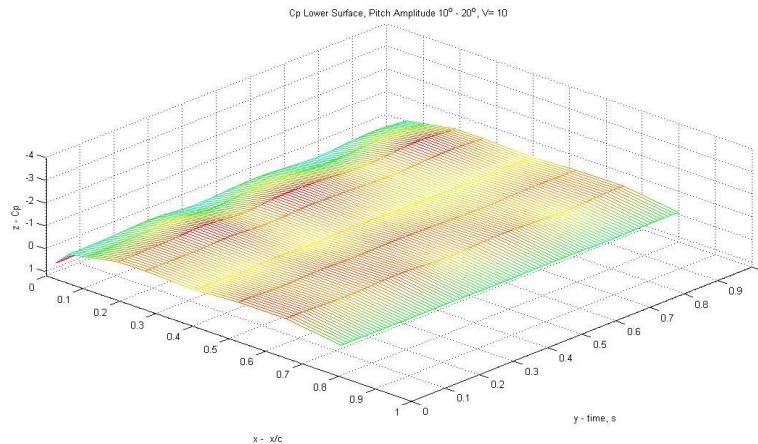


Figure 20: Variations of pressure coefficient with chordwise location on lower surface of NACA 0018 airfoil and time (Pitching amplitude =  $10^\circ - 20^\circ$ , Pitching frequency = 3 Hz, Free-stream velocity = 10 m/s)

Figure 19 and Figure 20 display the dynamic variations of pressure coefficient with chordwise location on upper and lower surfaces and time for pitching amplitude =  $10^\circ - 20^\circ$ , pitching frequency = 3 Hz and free-stream velocity = 10 m/s. Moving across the time, an unexpectedly large negative peak is observed on the upper surface. In comparison with other cases, it is known as the largest maximum suction with the attainment of peak magnitude as high as 3. In this instance, the vortex shed at the leading edge drives the formation of dynamic stall vortex, resulting in a substantial increase in peak magnitude. Upon increasing pitching amplitude and free-stream

velocity, the adverse pressure gradient on the upper surface also increases tremendously in a such way that it facilitates the separation of boundary layer.

Moving across the chordwise location, by inspecting the sinusoidal variation of pressure coefficient with time in Figure 19, the flow is expected to stall at  $x/c = 0.1$  in vicinity of the leading edge of the airfoil.

Similarly, the pressure variation on the lower surface is too small to yield any meaningful implications. The entire pressure coefficient stays constant for about a positive value.

In this instance, dynamic stall phenomenon possesses a profound impact on the wing pitching motion. Via dynamic stall, a strong vortex is created in vicinity of the leading edge namely leading edge vortex (LEV). The LEV then propagates over the upper surface until it approaches the trailing edge. When the LEV travels past the upper surface, the magnitude of lift increases to a great extent. In contrast to the static lift produced at the corresponding angle of attack, this increased lift is expected to be much greater. Nevertheless, the lift declines dramatically at the moment the LEV reaches the trailing edge.

#### **4. Conclusion**

The pressure distribution over the lower and upper surfaces of an airfoil is defined by a dimensionless quantity called pressure coefficient. At moderate angles of attack up to  $18^\circ$  angle of attack, the flow velocity is increasingly higher over the upper surface of the airfoil, leading to lower local pressure than free-stream pressure. Consequently, the resulting pressure coefficient exhibits a negative value across the upper surface. On top of that, there is a maximum suction peaking at minimum pressure coefficient in vicinity of leading edge on the upper surface, followed by a region of adverse pressure gradient.

Free-stream velocity is said to be the influential parameter for the peak suction. It can be deduced that as the free-stream velocity increases, the suction peak on the upper surface also grows larger. Apart from this, the peak suction and the adverse pressure gradient is highly dependent on the pitching amplitude. It can be inferred that higher angle of attack especially when the pitching amplitude varies from  $10^\circ$  to  $20^\circ$  tends to amplify the peak suction and the adverse pressure gradient. In this instance, the adverse pressure gradient on the upper surface is strong enough for the separation of boundary layer to occur, paving the way for the pressure variation across the upper surface to be negligible.

Dynamic stall is known as a non-linear unsteady aerodynamic effect which will lead to the evolution of the flow field. This destructive phenomenon is intimately associated with wing pitching motion. In other words, the occurrence of dynamic stall is primarily due to the rapid change in angle of attack of an airfoil. The rapid change can induce a leading edge vortex which travels downstream past the trailing edge. This strong vortex possesses high velocity airflows across the upper surface and hence increases the lift generated. Yet, there is a sudden loss of lift and decline in pitching moment when the vortex approaches the trailing edge as evidenced by the fact that the pressure variation is increasingly small in vicinity of the trailing edge of the airfoil.

## Acknowledgements

The author would like to express the greatest appreciation to Dr Norizham Bin Abdul Razak for his constructive comments and suggestions in sharpening the pitching wing design. Moreover, the author would like to convey the sincerest thank you to technicians of School of Aerospace Engineering notably Mr. Mahmud Bin Isa, Mr. Nor Ridwan Mohamed Yusof and Mr. Mohd Amir Wahab who are always ready to offer assistance and guidance if there is a need.

## References

1. Sai, K.P.M., *Design, Fabrication and Testing of Flapping Wing Micro Air Vehicle*. International Journal of engineering Research and Applications, 2016. **1**(6): p. 133-150.
2. Abdi, S., M. Mani, and F. Ajalli, *Unsteady surface pressure measurement on a pitching air foil*. HEFAT 2008, 2008.
3. Rahman, A.H.A., et al., *Aerodynamics of Harmonically Oscillating Aerofoil at Low Reynolds Number*. Journal of Aerospace Technology and Management, 2017. **9**(1): p. 83-90.
4. Knoller, R., *Die gesetze des luftwiderstandes*1909: Verlag des Österreichischer Flugtechnischen Vereines.
5. Betz, A., *Ein beitrage zur erklarung des segelfluges*. Zeitschrift fur Flugtechnik und Motorluftschiffahrt, 1912. **3**(1): p. 269-272.
6. Katzmayr, R., *Effect of periodic changes of angle of attack on behavior of airfoils*. 1922.
7. Von Karman, T. and J. Burgers, *Aerodynamic theory*. Berlin: Julius Springer, 1935. **2**: p. 52.
8. Theodorsen, T., *General theory of aerodynamic instability and the mechanism of flutter*. 1979.
9. Garrick, I., *Propulsion of a flapping and oscillating airfoil*. 1937.
10. McCroskey, W.J., *Unsteady airfoils*. Annual review of fluid mechanics, 1982. **14**(1): p. 285-311.
11. Ericsson, L. and J. Reding, *Unsteady flow concepts for dynamic stall analysis*. Journal of aircraft, 1984. **21**(8): p. 601-606.
12. Ajalli, F., M. Mani, and M. Soltani, *An experimental investigation of pressure distribution around a heaving airfoil*. HEFAT 2007, 2007.
13. Soltani, M., M. Mani, and E. Tolouei. *An Experimental Investigation of Surface Pressure Variation over an Oscillating Airfoil*. in *The 11th Australian International Aerospace Congress*. 2005.
14. McCroskey, W.J., et al., *Dynamic stall on advanced airfoil sections*. Journal of the American Helicopter Society, 1981. **26**(3): p. 40-50.
15. McAlister, K., et al., *An experimental study of dynamic stall on advanced airfoil section. volume 2: Pressure and force data*. 1982.
16. Fung, K.-Y. and L. Carr, *Effects of compressibility on dynamic stall*. AIAA journal, 1991. **29**(2): p. 306-308.
17. Koochesfahani, M.M., *Vortical patterns in the wake of an oscillating airfoil*. AIAA journal, 1989. **27**(9): p. 1200-1205.
18. Sarkar, S. and K. Venkatraman, *Numerical simulation of thrust generating flow past a pitching airfoil*. Computers & Fluids, 2006. **35**(1): p. 16-42.
19. Long, L.N. and T.E. Fritz, *Object-oriented unsteady vortex lattice method for flapping flight*. Journal of aircraft, 2004. **41**(6): p. 1275-1290.
20. Streitlien, K., G.S. Triantafyllou, and M.S. Triantafyllou, *Efficient foil propulsion through vortex control*. AIAA journal, 1996. **34**(11): p. 2315-2319.

21. DeLaurier, J. and J. Harris, *Experimental study of oscillating-wing propulsion*. Journal of aircraft, 1982. **19**(5): p. 368-373.
22. Razak, N.A. and G. Dimitriadis, *Experimental study of wings undergoing active root flapping and pitching*. Journal of Fluids and Structures, 2014. **49**: p. 687-704.
23. Tuncer, I., R. Walz, and M. Platzer. *A computational study on the dynamic stall of a flapping airfoil*. in *16th AIAA applied aerodynamics conference*. 1998.
24. Tuncer, I.H. and M.F. Platzer, *Computational study of flapping airfoil aerodynamics*. Journal of aircraft, 2000. **37**(3): p. 514-520.
25. Isogai, K., Y. Shinmoto, and Y. Watanabe, *Effects of dynamic stall on propulsive efficiency and thrust of flapping airfoil*. AIAA journal, 1999. **37**(10): p. 1145-1151.
26. Anderson, J., et al., *Oscillating foils of high propulsive efficiency*. Journal of Fluid Mechanics, 1998. **360**: p. 41-72.
27. Guglielmini, L. and P. Blondeaux, *Propulsive efficiency of oscillating foils*. European Journal of Mechanics-B/Fluids, 2004. **23**(2): p. 255-278.
28. Ramamurti, R. and W. Sandberg, *Simulation of flow about flapping airfoils using finite element incompressible flow solver*. AIAA journal, 2001. **39**(2): p. 253-260.
29. Read, D.A., F. Hover, and M. Triantafyllou, *Forces on oscillating foils for propulsion and maneuvering*. Journal of Fluids and Structures, 2003. **17**(1): p. 163-183.
30. Schouveiler, L., F. Hover, and M. Triantafyllou, *Performance of flapping foil propulsion*. Journal of Fluids and Structures, 2005. **20**(7): p. 949-959.
31. Ericsson, L.E. and J.P. Reding, *Dynamic stall of helicopter blades*. Journal of the American Helicopter Society, 1972. **17**(1): p. 11-19.
32. McCroskey, W., *Inviscid flowfield of an unsteady airfoil*. AIAA journal, 1973. **11**(8): p. 1130-1137.
33. Tran, C. and D. Petot, *Semi-empirical model for the dynamic stall of airfoils in view of the*. 1980.
34. Bielawa, R.L., et al., *Aeroelastic analysis for propellers-mathematical formulations and program user's manual*. 1983.
35. Akbari, M. and S. Price, *Simulation of the flow over elliptic airfoils oscillating at large angles of attack*. Journal of Fluids and Structures, 2000. **14**(6): p. 757-777.
36. Akbari, M. and S. Price, *Simulation of dynamic stall for a NACA 0012 airfoil using a vortex method*. Journal of Fluids and Structures, 2003. **17**(6): p. 855-874.
37. Wernert, P., et al., *Demonstration by PIV of the non-reproducibility of the flow field around an airfoil pitching under deep dynamic stall conditions and consequences thereof*. Aerospace science and technology, 1997. **1**(2): p. 125-135.
38. John, A.D. and J. Anderson, *Introduction to flight*, 1989, McGraw-Hill.